Simulation of laser multi-beam interference patterns for nanostructuring of materials

Gerhard Liedl[1], Robert Pospichal[1]

[1]Vienna University of Technology, Institute for Production Engineering and Laser Technology, Gusshausstraße 30, Vienna, Austria

Corresponding author: gerhard.liedl@tuwien.ac.at

Nanostructuring of materials has developed into an interesting possibility for the modification of surfaces. As an example, biomimetic surfaces with ordered structures in the nanometer range show super-hydrophobicity or self-cleaning properties. Several different production methods exist, like nanoimprint lithography or electron beam lithography and others. Compared to other well established production methods, laser interference lithography (LIL) is a single-step process which combines high efficiency with relatively low fabrication costs. As a non-contact processing tool, LIL is able to ablate different materials, like polymers, metals and even ceramics without tool wear. Furthermore, ultra-short pulse laser systems allow processing of moving workpieces without any motion blur due to the short interaction time. In any case, LIL patterning of materials in order to mimic biological surfaces requires the interference of at least two laser beams with well defined orientation, polarisation, phase relation and intensity. Periodicity of the intensity distribution depends on the wavelength and the angle between interfering laser beams. Depending on desired surface structures, interference of two or more laser beams is needed to generate the required intensity distribution for nanostructuring of surfaces. Emanating from biological multi-functional surface structures, different laser beam configurations have been calculated to customize interference patterns for the production of biomimetic surfaces. Examples of surface profiles with hydrophobic behavior have been taken from the literature. In a next step, laser intensity distributions have been calculated which mimic inversely the desired structures. It is assumed that the calculations will help to reduce the number of required experiments significantly.

Keywords: laser, interference, nanostructuring

Introduction

During the last years, biological surfaces have been studied extensively in many different aspects. It is well known that surfaces of plants act as multifunctional interfaces to the environment. Adapted to conditions ranging from hot and arid regions to wet and aquatic environments plants have developed strategies to protect themselves against harmful radiation or against contamination. Especially such self-cleaning properties have gained wide-spread interest due to the range of possible applications. As an example, the leaves of the lotus plant with their extremly water-repellent behavior inspired researchers world-wide and have been the origin of several already existing industrial applications and patents.

Water repellent or hydrophobic surface structures of plants show a more or less hierarchical structure. The surface usually consists of small convex shaped surface cells which are covered with three-dimensional wax crystals with sizes ranging from 0.5 µm up to 20 µm [1], [2]. If the surface of such plants is contaminated with particles, a water droplet collects the particles and removes it when it rolls of the surface [2].

A water droplet on a hydrophobic surface shows a certain contact angle and hydrophobicity is established if the contact angle exceeds 90°. Superhydrophobic surfaces show contact angles larger than 150°, whereas contact angles less than 90° are characteristic for hydrophilic surfaces. Additionally, if a water droplet rolls of a surface at even low tilting angles, it is assumed that the surface provides self-cleaning properties, see Fig. 1.

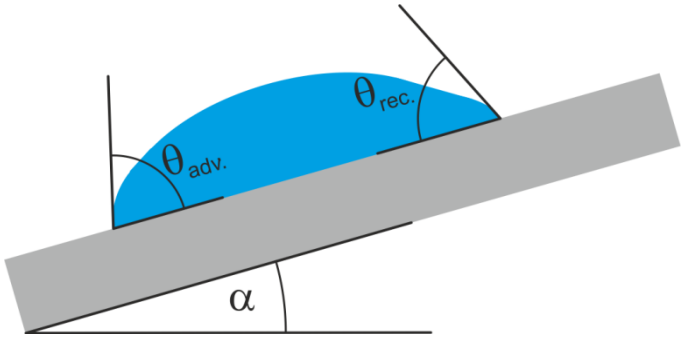

Fig. 1: Contact angle Θ and tilt angle α. Hysteresis of the contact angle is defined as difference between advancing or receding contact angles $\Theta_{adv.} - \Theta_{rec.}$ of a water droplet and is responsible for „sticking“ of liquids on surfaces [3]. Self-cleaning surfaces show small tilt angles [4].

Many surfaces of plants show a self-cleaning abilities which protects plants against pollu tion. Barthlott and others authors [5], [6] identified a large variety of plants which show hydrophobicity and self-cleaning properties. It is assumed that the effect is based on two principles [3]. Examples of self-cleaning plants in nature show a hydrophobic surface, the so called cuticula, which consists in most cases of a wax layer. This layer increases the interface tension between the leaf and the water droplet. As a consequence, the contact angle between surface and water droplet increases, too. It has been shown that it is possible that such wax layers may erode during plant growth, leaving plant surfaces almost smooth and without water-repellent properties [2]. The other main effect is based on a hierarchical surface structure. Burling-like structures (papillae) are placed on the cuticula. The burling extent to a height up to several microns and placed at a distance between 10 µm and 15 µm next to each other. These papillae exhibit finer structures on their surfaces, where the actual nano-structure is superimposed by means of wax crystals. Usually, these crystals show diameters in the order of 100 nm. Several studies have proved that a correlation between the existence of a two-part surface structure and the super-hydrophobic behavior exists. On the other hand, it has been shown that examples in nature exist, which exhibit one-part surface structures in the nanometer range with excellent super-hydrophobic behavior [2]. In any case, the contact area between water droplet and surface is minimized as well as adhesive forces. As a consequence, water droplets on the surface take a more or less spherical from. The contact angle between droplet and surface is used to characterize the hydrophobicity of surface structures.

Different approaches to produce nano-structures on a large variety of materials have been developed during the last years. In most cases, methods can be divided into top-down or bottom-up processes. Bottom-up processes use chemical or physical forces to assemble small units into larger structures, for example chemical vapor deposition or phase separation. In top-down processes, larger structures are manipulated for example with lithographic methods. Both possibilities have been described for example by Roach et al. or Bhushan et al. [7], [3].

Laser-workpiece interaction

Laser material processing is an additional possibility for the generation of nano-structures on materials. Material processing with short and ultra-short laser beams offers new possibilities in modifying surface structures of a wide range of different materials. Metals as well as ceramics, glasses or organics materials can be processed without significant damage. In contrary, processing with long pulses or continuous wave lasers causes significant damage and more or less pronounced heat affected zones (HAZ). In contrary to micro processing of materials, such HAZ are usually negligible in macro processing whereas in micro processing material damage of non-irradiated regions should be minimized.

Heat conduction requires a certain amount of time to transport heat from a layer irradiated by a laser pulse into the bulk of the material. With decreasing pulse duration the heat flow becomes more and more insignificant and other effects dominate. Typically, with picosecond or even sub-ps laser pulses the interaction of the irradiated material and the incoming electromagnetic wave has to be taken into account. Only after a certain, material dependent time span the thermalization of the bulk material dominates. On shorter time scales the incoming electromagnetic wave interacts with the electrons within the material. Due to the fact that the electron mass is much lower than the atom mass, the electrons follow almost immediately the electromagnetic wave. Since in metals free electrons are available whereas in dielectrics no free electrons are available, the first few moments in the interaction are different between metals and dielectrics. As a consequence, the macroscopic behavior is identical for metals and dielectrics or semiconductors for long laser pulses, whereas at shorter timescales material responses to short pulses are totally different. Additionally, irradiation regimes influence ablation rates.

In the following a model proposed by Gamaly et al. and other authors of the interaction of an ultra-short laser pulse with matter will be discussed briefly. Depending on the optical properties of the material the incoming electromagnetic wave is transmitted to a certain amount into the bulk of the material. Electrons begin to oscillate and accumulate energy from the laser radiation. With weak electromagnetic fields and long pulses, the electrons will collide with the atoms in the lattice and energy is transferred to the lattice, causing heating of the lattice and the well-known thermal effects of laser radiation. Usually, the time required to reach a thermal equilibrium between lattice and electrons is in the order of picoseconds up to tens of picoseconds [8], [9].

For description of the interaction between a metal and an electromagnetic wave which causes material removal a “two-temperature-model” is used. The main idea that ultra-short pulses with sub-ps duration interact with the electrons first and the lattice itself remains cold. As a consequence, the temperature of the free electron gas is different from the temperature of the lattice. Since the electrons react much faster on the incoming electromagnetic wave, their temperature will rise almost immediately to extremely high values, whereas the lattice temperature remains unchanged. Electron and lattice temperatures are described with two coupled differential equations, where coupling between electrons and the lattice is introduced with an electron-lattice coupling coefficient. For longer pulses a thermal equilibrium between electrons and the lattice is reached during the duration of the pulse [8].

Due to the much larger heat conductivity of the electrons, the conductivity of the lattice can safely be ignored for ultra-short pulses. Almost immediately after the onset of the laser pulse, the electron gas will reach very high temperatures whereas the lattice temperature remains unchanged.

Depending on the material and the laser fluence, the interaction between electron gas and lattice heats the lattice within several up to tens of picoseconds. After that a thermal equilibrium between electron gas and lattice is established. Expected ablation depths have been calculated to depend logarithmically on the ratio between laser fluence and threshold fluence [8]:

$$\Delta z = \frac{1}{\alpha} ln\left(\frac{F}{F_{th}}\right)$$

with a threshold fluence F_{th}. Recently, a linear dependence of the ablated depth on the fluence has been proposed for high fluence regimes [10]. Since the deviations are relatively small we will continue with the logarithmic description.

Dielectric materials show a different behavior. Since no free electrons are available, they have to be generated by the process. Acceleration of free electrons causes a multiplication and the electrons are heated by the incoming laser pulse. As a consequence, the previous dielectric material starts to behave like a metal. Emission of electrons from the surface changes the electric charge of the remaining material and strong repulsive forces can cause strong emission of ions. Regarding longer timescales, differences in the material behavior between metals and dielectrics are vanishing [9].

As a consequence, the generation of free electrons is of crucial importance in a description of a dielectric material in response to an ultra-short laser pulse. Free electrons can interact with the electromagnetic wave via inverse bremsstrahlung and accumulate energy. The atoms remain totally unaffected during the pulse. It has been shown by Gamaly et al. that electron density, skin depth, absorption and collision frequency remain approximately constant almost immediately after the onset of the laser pulse and a skin effect approximation can be used to describe the interaction between laser pulse and target [11].

Gamaly et al. presented a simplified model of the interaction between intense laser pulses and materials [12]. At high intensities in the range of 10^{14} W/cm^2 almost any material is ionized immediately. As already mentioned, relaxation times are much longer compared to the pulse duration and almost no hydrodynamic motion occurs on a femtosecond time scale. Due to the fact that relevant material parameters change during the laser pulse, solutions for the coupled electrical fields and material equations are quite complicated. Gamaly et al. [11] proposed an exponential decay within the material

$$E(z) = E(0)e^{-z/l_s}$$

with l_s as the skin-depth.

The plasma frequency which is defined as

$$\omega_p = \left(\frac{n_e e^2}{\varepsilon_0 m_e}\right)^{1/2}$$

can be used to define the start of material removal. When the plasma frequency is close to the frequency of the incoming laser radiation, optical properties change dramatically [13], [14]. The number density of electrons which influences the plasma frequency depends on the interaction of

the laser beam with the irradiated material. In dielectric materials no free electrons are available and free electrons have to be generated by the laser pulse. At low fluences and in weak absorbing media impurities or doping materials can change the absorption behavior fundamentally [15].

At higher fluence regimes the influence of a strong electromagnetic field causes ionization of the material and the number density of free electrons can be described by a rate equation

$$\frac{dn_e}{dt} = n_0 w_{mpi} + n_e w_{imp}$$

where n_0 is the number of neutral atoms, w_{imp} is the impact ionization probability and w_{mpi} is the probability for multiphoton ionization. Depending on the intensity, either multiphoton ionization or impact ionization dominates the ionization process [9].

Gamaly et al. describe an approximation for relation of the absorption coefficient and the skin depth as

$$\frac{A}{l_s} \approx \frac{2\omega}{c} = \frac{4\pi}{\lambda}$$

with the absorption A from the Fresnel formula as

$$A = 1 - R \approx \frac{4n}{(n+1)^2 + n^2}$$

[9].

Following the first ionization step of an irradiated sample free electrons interact with the remaining laser pulse. Since the ionization time is in the order of a few femtoseconds, absorption of the subsequent laser pulse is identical to the one of free electrons in metals.

Depending on the relation between the pulse duration and the thermal relaxation times and absorbed energy Gamaly et al. described the emission of energetic electrons from the surface of the sample which leave the sample and create a strong electric field. If the field strength is high enough, ions can be pulled out of the sample and an electrostatic ablation occurs. It has been shown by Gamaly et al. that the time scale for an ion to acquire enough energy to leave the sample is in the order of the pulse duration or even shorter [12].

As already mentioned, the ablation threshold fluence separates different regimes where

$$\Delta z = \begin{cases} 0 & F \le F_{th} \\ \frac{1}{\alpha} \ln\left(\frac{F}{F_{th}}\right) & F \ge F_{th} \end{cases}$$

with the absorption coefficient α related to the skin depth [11].

As an example, sub-ps lasers emit radiation with pulse energies of several up to tens of µJ at repetition rates of several 100 kHz up to MHz with an average power of several Watts. Typically, the

emitted wavelength is approx. 1 µm, with the possibility to use higher harmonics in the visible or in the ultraviolet range of the spectrum. The intensity of a laser with a pulse energy of several ten µJ and a pulse duration in the range of 100…300 fs, focused to a spot with a diameter of 100 µm calculates as:

$$I \approx 2 \cdot 10^{15} \ldots 5 \cdot 10^{16} \left[W/m^2 \right]$$

The field strength is related to the intensity

$$E = \sqrt{\frac{2 \cdot I}{\varepsilon_0 \cdot c}}$$

In the case of a plane electromagnetic wave the intensity is the power of the beam divided by the beam area, whereas a beam with a Gaussian distribution gives a peak intensity twice the average intensity of the beam.

Ablation by short laser pulses

As mentioned previously, interaction between electromagnetic radiation and matter involves acceleration of electrons. Since we are focusing on ultra-short time scales, there is almost no influence on the atoms during the duration of the laser pulse. Laser beam intensities in the order of 10^{13} - 10^{14} W/cm^2 are able to ionize any material immediately after the onset of the laser pulse. After that, heating of the sample takes place independently of the initial state of the material.

According to that, the ablation threshold is different for metals and dielectric materials. For metals, the free electrons have to overcome the work function, whereas for dielectrics a certain number of free electrons have to be generated first. Following that electrons which have gathered sufficient energy to escape the sample create a strong electric field. The field strength depends on the energy of the electrons and the gradient of the electron density perpendicular to surface of the sample [11].

For dielectric materials, a certain amount of energy E_I is required to transfer electrons from the valence band into the continuum. In order to remove ions from the material an additional energy E_B is required. Gamaly et al. described the threshold fluence for ablation as [9]

$$F_{th}^{d} = \frac{3}{4}\left(E_B + E_I\right)\frac{l_s n_e}{A}$$

For metals the ablation threshold can be estimated where the electrons have to overcome the work function as

$$F_{th}^{m} = \frac{3}{4}\left(E_B + E_{esc}\right)\frac{l_s n_e}{A}$$

At timescales of ultra-short laser pulses, the threshold fluence for ablation of metals is lower than that for inorganic dielectric materials.

Depending on the intensity, incubation effects for transparent materials have to taken into account, where first pulses initiate following ablation. As a consequence, ablated depth differs for single or

multiple pulse exposures. Regarding polymers, experimental results indicate that ablation thresholds increase with increasing pulse duration for PMMA with a strong incubation behavior for ultra-short pulses [16]. Incubation modifies the ablation threshold in such a way that increasing pulse numbers cause a decrease of the threshold fluence of N laser pulses

$$F_{th}(N) = F_{th}(1) N^{\xi-1}$$

[17], typically, the incubation parameter ξ ranges from 0.6 up to 0.9. For estimating ablation of polymers we will focus on single pulse ablation.

An estimation of threshold fluences of polymers according to the model proposed by Gamaly et al. for dielectric materials gives threshold fluences in the range between 0.5 and up to 2 Jcm^{-2} [9]. Experimental values measured by Baudach gives ablation threshold fluences in the range 1.0 up to 2.6 Jcm^{-2} [18].

Laser beam interference

In most cases, laser material processing uses a focused laser beam for material removal where the diameter of the focused laser beam depends on the wavelength of the radiation. Material removal with µm and sub-µm resolution with a focused laser beam is time-consuming and will not be discussed here. Instead of that, interference of coherent radiation can be used to create nanostructures on the surface of materials.

Interaction of at least two coherent electromagnetic waves at a certain angle between each other causes a so-called “interference pattern”. The resulting interference pattern not only depends on the angle between each wave but on polarization and phase relation, too [19]. Superposition of two or even more monochromatic, plane electromagnetic waves leads to

$$E = \sum \vec{E}_{0,j} \cdot e^{-i\left(\vec{k}_i \cdot \vec{r} - \omega t + \phi_i\right)}$$

And since the resulting intensity I is proportional to

$$I \propto |E|^2$$

the intensity includes interference terms. Polarisation $\vec{E}_{0,i}$, direction of propagation $\overrightarrow{k_i}$ and phase relation ϕ_i between individual waves influence the resulting interference pattern.

The resulting intensity of a superposition of n electromagnetic waves can be written as

$$I_{Total} = \sum_i I_i + \sum_{i<j} \vec{E}_{0,j} \cdot \vec{E}_{0,j} \cos\left(\left(\vec{k}_i - \vec{k}_j\right) \cdot \vec{r} + \phi_i - \phi_j\right)$$

The second term on the right hand side describes the interference between n waves. As can be seen, the interference term vanishes in the case of perpendicular polarization and only the sum of single intensities remains. Phase differences and different propagation vectors alter the resulting interference pattern. As an example, interference of two electromagnetic waves with identical polarization propagating in x and –x direction creates a periodic interference pattern with a spacing

of $\lambda/2$. Interference of three or more beams generates two- or even three-dimensional patterns, see Fig. 2.

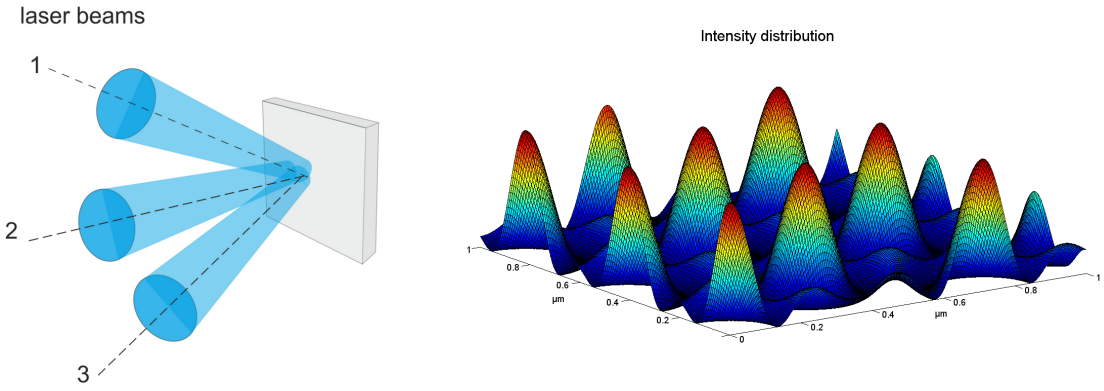

Fig. 2: Schematical view of three interfering laser beams (left). Resulting intensity distribution of interfering beams (right) with identical polarization orientation and amplitude.

Modification of polarization, phase shift and angle of incidence changes the resulting interference patterns. As an example, the resulting intensity distribution of an interference of 4 laser beams with and without phase shift between two beams is shown in Fig. 3.

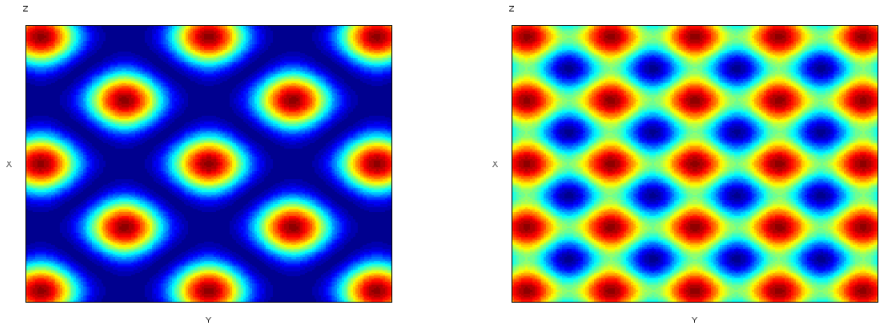

Fig. 3: Calculated intensity distribution of four interfering laser beams at the surface of a sample. Z-axis perpendicular to the paper plane. Beams are symmetrically distributed around the z-axis and at angle of 35° from the z-axis. Orientation of polarization identical for all four beams. Left: No phase shift between individual beams. Right: 90° phase shift between beam 1 and beam 3.

Changing the polarization orientation of the beams changes the resulting intensity distribution, too. The following examples show calculated intensity profiles for different interference conditions. Estimated ablation regions have been chosen as 50% maximum intensity of the calculated intensity in the plots, examples are shown below, see Fig. 4.

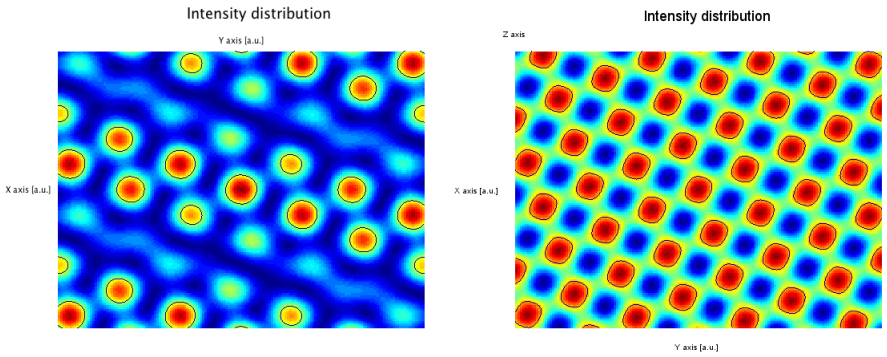

Fig. 4: Intensity distribution of 4 interfering laser beams. Left: Asymmetrical arrangement of the beams around z-axis. Right: Asymmetrical arrangement with different polarisation of 2 beams.

It has been shown by different authors that interference of laser beams can be used to structurize dielectric materials and even metals, for example [20], [21] , [22], [23], polymers have been structured by Berendsen et al., Wu et al. or Lasagni et al. [24] , [25], [26]. Laser interference pattering has been recognized as a valuable tool to structurize a large variety of materials in the sub-µm range.

Although lasers which emit ultra-short pulses are available with pulse frequencies up to several 100 kHz, areas which can be processes within reasonable time are quite limited. As an advantage, due to the short interaction time, processing of moving samples should be possible without any motion blur. For example, a laser with a pulse frequency of 100 kHz and a focus diameter of 100 µm structurizes less than 1 mm^2 per second. On the other hand, structuring of individual textile fibers during production would allow a velocity of the fiber of 10 m/s without additional measures.

Summary and Outlook

Interference of multiple laser beams is able to produce regular patterns on substrates with feature sizes in the sub-µm range. Depending on the number of interfering beams, their orientation, polarization and phase shift resulting structures can be tailored according to the needs for super-hydrophobicity. Short pulse durations together with high repetition rates offer the possibility to process sample areas of several mm^2 per second. Processing of polymer materials can be used to modify the wetting behavior and self-cleaning properties of textile materials. Due to the extremely short interaction time together with high pulse repetition rates even nano-structuring of single threads seems within reach. Structuring of textile fibers provides an opportunity to produce textiles with built-in hydrophobic properties.

As a next step, according to the calculated requirements of a laser source different laser systems will be evaluated. Although calculation of interference patterns is a simple possibility to design intensity distributions according to the requirements for generation of hydrophobic surfaces, an experimental verification is essential. Additionally estimated ablation thresholds should be critically reviewed and experimental values should be used to modify the assumptions used for the calculations of ablation. In an additional step, experimental verification of ablation rates of materials used for the production of textiles is intended. Consecutively, the feasibility of laser structuring of single textile fibers should be evaluated.

References

[1] C. a. B. W. Neinhuis, Annals of Botany, 97 (1997).
[2] K. Koch, B. Bhushan, and W. Barthlott, Progress in Materials Science **54,** 2 (2009).
[3] B. Bhushan and Y. C. Jung, J. Phys.: Condens. Matter **20,** 22 (2008).
[4] D. Öner and T. J. McCarthy, Langmuir **16,** 20 (2000).
[5] W. Barthlott *et al.*, Adv. Mater. **22,** 21 (2010).
[6] B. Bhushan, K. Koch, and Y. C. Jung, Appl. Phys. Lett. **93,** 9 (2008).
[7] P. Roach, N. J. Shirtcliffe, and M. I. Newton, Soft Matter **4,** 2 (2008).
[8] D. Bäuerle, *Laser Processing and Chemistry, 4th Edition* (Springer, 2011).
[9] E. G. Gamaly, A. V. Rode, and B. Luther-Davies, in *Pulsed laser deposition of thin films. Applications-led growth of functional materials, in:*edited by R. Eason (Wiley-Interscience, Hoboken, N.J, 2007).
[10] P. Balling, B. H. Christensen, J. Byskov-Nielsen, and D. Q. S. Le, in *Proceedings SPIE, in:*edited by SPIE (2008).
[11] E. G. Gamaly, A. V. Rode, B. Luther-Davies, and V. T. Tikhonchuk, Phys. Plasmas **9,** 3 (2002).
[12] E. Gamaly, A. Rode, V. Tikhonchuk, and B. Luther-Davies, Applied Surface Science Vol. **197-198** (2002).
[13] M. von Allmen and A. Blatter, *Laser-beam interactions with materials. Physical principles and applications* (Springer, Berlin ;, New York, 1995).
[14] B. Christensen and P. Balling, Phys. Rev. B **79,** 15 (2009).
[15] T. Lippert and L. Urech, in *Photochemistry and photophysics of polymer materials, in:*edited by N. S. Allen (J. Wiley, Hoboken, N.J, 2010).
[16] J. Krüger *et al.*, Applied Surface Science **247,** 1-4 (2005).
[17] J. Krüger and W. Kautek, in *Advances in Polymer Science, in:*edited by T. K. Lippert (Springer Berlin Heidelberg, Berlin, Heidelberg, 2004).
[18] S. Baudach, PhD, 2001.
[19] E. Hecht, *Optics* (Oldenbourg, München ;, Wien, 1999).
[20] C. Tan *et al.*, Nanotechnology **20,** 12 (2009).
[21] M. D'Alessandria, A. Lasagni, and F. Mücklich, Applied Surface Science **255,** 5 (2008).
[22] M. Tang, M. Hong, and Y. Choo, in *2008 IEEE PhotonicsGlobal at Singapore, IPGC 2008, 2008, 2008 IEEE PhotonicsGlobal at Singapore, IPGC 2008, in:*edited by IEEE (2008).
[23] C. Daniel, F. Mücklich, and Z. Liu, Applied Surface Science Vol. **208-209** (2003).
[24] A. Lasagni *et al.,* in *Proc. SPIE, in:*edited by Ángel B. Rodríguez-Vázquez (2010).
[25] C. W. Berendsen, M. Škereň, D. Najdek, and F. Černý, Applied Surface Science **255,** 23 (2009).
[26] L. Wu *et al.*, Applied Physics Letters **86,** 24 (2005).